INVESTIGATION OF SUPERSONIC AND HYPERSONIC SHOCK-WAVE/BOUNDARY-LAYER INTERACTIONS

R.O. Bura, Y.F. Yao[1], G.T. Roberts and N.D. Sandham
Aerodynamics & Flight Mechanics Research Group
School of Engineering Sciences
University of Southampton
Southampton SO17 1BJ, UK
E-mail: R.O.Bura@soton.ac.uk

Abstract

Numerical simulations of 2-D supersonic and hypersonic laminar shock-wave/boundary-layer interactions (SBLIs) have been carried out by solving the Navier-Stokes (NS) equations using a compressible flow code over a wide range of Mach numbers and shock strengths. The results obtained at Mach 2.0 and 7.87 were compared with experimental data. At Mach 2.0 the simulated pressure and skin friction distributions in the interaction region agreed well with the experimental data and results of other numerical simulations. At Mach 7.87 the simulation results compared less favourably with the available pressure and heat-flux data. Possible causes of these discrepancies are proposed and discussed. In addition, the numerical data were further analysed by means of correlation laws derived by previous researchers, but here extended to higher Mach numbers. A correlation of peak heating data has also been performed.

Keywords

Shock-Wave/Boundary-Layer Interactions.

1. Introduction

The interaction of shock waves with developing boundary-layer flows occurs in many practical situations at transonic, supersonic and hypersonic speeds. Often the interaction results in boundary-layer separation with downstream re-attachment. As a result, significant changes occur in the aerodynamic and thermal loads, when the shock is strong. Shock-wave/boundary-layer interactions (SBLIs) are of special importance in hypersonic flows, since they can result in extremely high local heat-fluxes. Regions of particular concern are at wing-body or fin-body junctions, on deflected control surfaces (e.g. compression ramps) and near intakes on vehicles employing airbreathing propulsion. This problem is critical for the correct sizing of thermal protection systems (TPS) in parts of the vehicle where such interactions are likely to occur.

Due to the complexity of the phenomena involved, elucidation of the flow physics and accurate estimation of the pressure and heating levels generated in such interaction regions are extremely difficult. Consequently TPS designs are typically conservative. This inevitably results in over-protection, leading to reduced payload capacity, reduced performance, higher costs and possibly even reduced reliability (Holden, 1986). Thus it remains an important goal to understand fully the flow phenomena associated with SBLIs.

In the present study, results from a numerical investigation of a spatially-developing steady 2-D laminar boundary-layer over a flat plate interacting with an oblique shock-wave are presented. The study is intended to be a precursor of 3-D, unsteady simulations of a SBLI flowfield in which perturbations are introduced in order to determine the boundary-layer stability and its propensity to undergo transition. The motivation for this work is the measurement of unexpectedly high heat-fluxes on a compression ramp in a nominally 2-D laminar hypersonic SBLI flowfield in experiments performed at the University of Southampton by Smith (1993). Similar anomalously high heat-fluxes in 2-D hypersonic flows with separation have also been reported by other workers (Delery and Panaras, 1996). There are several possible mechanisms for the observed enhanced heat-fluxes, one being shock-induced transition in the separated shear layer.

Since the first observation of the SBLI phenomenon about fifty years ago, significant progress has been achieved, both experimentally and computationally. Reviews of work carried out have been given previously by Hankey and Holden (1975), Adamson and

[1] Present address: Demag Delaval Industrial Turbo-machinery Ltd., PO Box 1, Waterside South, Lincoln LN5 7FD, UK

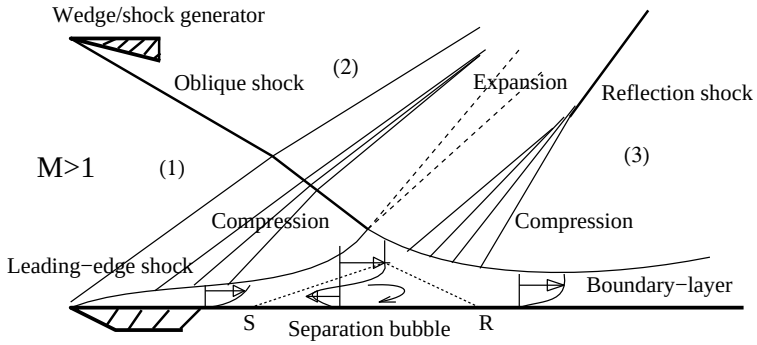

Figure 1: A sketch of laminar shock/boundary-layer interactions with $M > 1$ inflow.

Messiter (1980), and most recently by Delery (1999) and Dolling (2001). The work has covered a wide range of Mach numbers and Reynolds numbers, and several different SBLI configurations. An important finding from this work is that, for given freestream conditions, the surface properties (pressure, shear stress and heat-flux) are primarily dependent on the overall pressure rise experienced in the interaction, irrespective of how this pressure rise is generated. Thus SBLIs arising from oblique shock impingement or from compression ramps have similar surface distributions of these properties; this, in turn, led to the *free interaction* concept, first proposed by Chapman *et al.* (1957).

Figure 1 illustrates a representative SBLI caused by the interaction of an incoming oblique shock-wave generated by a sharp wedge (shock generator) with a spatially-developing two-dimensional boundary-layer on a flat plate. This configuration contains the essential flowfield features typical of all 2-D oblique SBLIs and has been studied extensively, both experimentally and numerically, including this present work. The subscripts (1) and (2) denote the inviscid region in front of and behind the impinging shock, while the subscript (3) denotes the inviscid region behind the shock reflection downstream of the interaction. Also illustrated is a leading edge shock. With a supersonic freestream flow this feature will be weak if the flat plate has a sharp leading edge and is at zero incidence, but may not be under hypersonic flow conditions due to viscous interaction (Korkegi 1971).

For a given freestream Mach number, M_∞, the strength of the impinging oblique shock-wave, represented by the shock angle β, is controlled by the wedge angle θ. The viscous boundary-layer encountering the pressure increase p_3/p_1 across the interaction region is decelerated and thickened, and will separate if the shock is sufficiently strong (the zero skin friction point is denoted as 'S'). As illustrated, the influence of the impinging shock extends upstream of the impingement point. The impinging shock is usually reflected as an expansion fan, thus turning the flow towards the wall where the flow re-attaches (at the re-attachment point denoted as 'R'). Consequently, a primary separation bubble is formed. Two compression zones, extending from the separation and re-attachment regions, cause the pressure increase at the beginning and the end of the interactions. Over the separation region there is a flattened pressure variation, hereafter referred to as the 'pressure plateau'.

The general qualitative aspects of the interaction, as described above and illustrated in Fig. 1, applies to laminar, transitional and turbulent SBLIs, but the scale and severity of the interaction depend on the state of the boundary layer. In particular, as laminar boundary layers are more prone to separation, the extent of the interaction is much greater for laminar than turbulent boundary layers, and the pressure plateau is more pronounced. On the other hand, surface properties such as skin friction and heat transfer are much greater in transitional and turbulent interactions.

In most practical supersonic flow situations, the boundary-layer ahead of the SBLI is turbulent. However, for hypersonic flows at high altitude, fully laminar and transitional (laminar-turbulent) interactions can exist in continuum flow. In this paper, we limit the discussion to the flow configuration of an oblique shock interacting with a spatially-developing 2-D laminar boundary layer. As the flow configuration involves shock waves and flow separations, two of the most difficult features to reproduce numerically, it has become an important test benchmark for validating new numerical methods. Also, because of its laminar character, it carries no flow uncertainty associated with turbulence modelling that may influence the solution.

Pioneering experiments for this flow configuration were carried out by Chapman, Kuehn and Larson (1957) and Hakkinen et al. (1959), who advanced the earlier experimental work of Liepmann (1946) and provided the basic physical understanding of SBLI phenomena in the two-dimensional laminar flow regime. The flow conditions for their work were $M_\infty = 2.0$ and $Re \simeq 2.9 \times 10^5$. These experiments were also simulated numerically by Katzer

(1989) and Wasistho (1998), and provide a supersonic flow benchmark for the simulations presented in this paper. Degrez, Boccadoro and Wendt (1987) re-visited the problem for $M_\infty = 2.15$ and $Re \simeq 10^5$, aiming for a complete experimental database by using more advanced measurement techniques. A complementary numerical solution was also performed in their study.

Several experimental studies of 2-D laminar oblique SBLIs in the hypersonic regime have also been carried out, with Mach numbers ranging from 7.3 to 18.9 and Reynolds numbers from 1×10^5 to 25×10^5 (e.g. Needham and Stollery (1966), Kaufman and Johnson (1975) and Holden (1978)). Three-dimensional effects were investigated by Henckels et al. (1993) and Kreins et al. (1996) using high resolution surface measurement techniques, in which the existence of longitudinal Görtler vortices was observed in the flowfield downstream of the SBLIs. These experiments were carried out at Mach numbers of 6 and 8.7 with Reynolds number of approximately 9×10^5.

Numerical investigations of laminar hypersonic SBLI problems have also been carried out by Hodge (1977) and by Issa and Lockwood (1977). In general, the results agreed well with the wall pressure and heat-flux distributions for weak interactions, but not for strong interactions. Domröse et al. (1996) carried out 2-D and 3-D numerical simulations, aiming for re-producing the experiment by Henckels et al. (1993). In these numerical simulations, Görtler vortices were observed downstream of the re-attachment line.

The 2-D numerical simulations carried out in this present study cover a broad range of Mach numbers, from supersonic to hypersonic (see Table 1). Reynolds numbers were sufficiently low to ensure that the boundary-layer boundary-layer growing over the flat plate in the absence of the SBLI remained laminar. The overall pressure ratio p_3/p_1, governed by the impinging shock strength, was treated as a variable parameter. Where possible, the results are compared with experimental and/or other numerical results. The results are also analysed in terms of correlation parameters proposed by Katzer (1989), derived from the earlier work by Chapman *et al.* (1957).

Table 1: Parameter combinations of numerical investigation

Case	Symbols	Mach number, M_∞	Reynolds number, $R_{e_{x_o}}$	Overall p. ratio (p_3/p_1)
1	Δ	7.87	1.48×10^6	5.41
2	∇	7.73	0.46×10^6	1.56; 3.08; 5.56
3	$\triangleright$	6.85	0.78×10^6	11.00
4	$\triangleleft$	6.85	0.25×10^6	2.68; 4.56; 7.33; 11.08
5	$\diamond$	4.50	0.30×10^6	1.74; 2.91; 4.43
6	$\circ$	2.00	0.30×10^6	1.25; 1.40; 1.63; 1.86

2. Numerical Method

A complete description of the numerical method used in the present study was given by Sandham et al. (2002) for a shock-free compressible turbulent channel flow. Using this code the compressible unsteady 3-D Navier-Stokes (NS) equations are solved via a 4th-order central finite-difference-TVD scheme for evaluating spatial derivatives and an explicit 3-step Runge-Kutta algorithm for time advancement. Other numerical techniques are also used, including entropy splitting of Euler terms, a Laplacian form for viscous terms and a stable high-order boundary treatment. A Sutherland law viscosity variation is implemented with thermal conductivity evaluated via a fixed Prandtl number (0.72 for air and 0.70 for nitrogen). The fluid is assumed to behave as a thermally perfect gas with constant specific heat capacities in the ratio $\gamma = 1.4$.

Yao et al. (2000) have demonstrated the capability of the same numerics for flows containing shock waves and preliminary results of some of the present oblique SBLI simulations have also been presented elsewhere (Bura *et al.* (2001) and Yao *et al.* (2002)). The code has been developed specifically to investigate transitional/turbulent boundary-layer phenomena by direct numerical simulation (DNS). In the work presented here, however, discussion is limited to steady, laminar SBLI simulations in 2-D. The solution is advanced in time until steady-state conditions are achieved, as evidenced either by a rate of change of wall pressure less than 10^{-6} per time step, or until there were negligible changes in the flow properties of primary interest, such as separation lengths and wall shear stress and heat-flux.

Time advancement was limited by stability requirements, the maximum CFL used being 2.0 for cases 1-4 (hypersonic inflow) and 2.0 for cases 5-6 (supersonic inflow). Convergence to a steady state required more iterations as the shock

angle (corresponding to shock strength) was increased. This, in turn, increased the number of time units (non-dimensional time) required for the solution to converge to a steady state. A typical strong shock case ($M_\infty = 6.85$) took 300,000 iterations ($\sim$ 8000 time units) to converge. For all computations, both supersonic and hypersonic cases, the codes used were configured to run on single processor (SGI Origin 2000 computer).

2.1 Input and boundary conditions

For each of the test cases considered in Table 1, the computational domain comprised a rectangular box, arranged in such a way that the oblique shock originated from near the top left hand of the upper boundary and impinged near the middle of the lower (solid wall) boundary. The $M_\infty = 2.0$ simulation (case 6) is a repeat of that carried out originally by Katzer (1989) and Wasistho (1998), and is based on experiments performed by Hakkinen *et al.*. This simulation was used as a benchmark. Hypersonic SBLI simulations were also carried out at Mach numbers of $M_\infty \sim 8.0$ (cases 1 and 2) and $M_\infty = 6.85$ (cases 3 and 4). The former were based on experiments performed by Kaufman and Johnson (1974), and the latter conditions were similar to those employed by Smith (1993) in his compression ramp experiments at the University of Southampton. The $M_\infty = 4.5$ simulation (case 5) was used as an intermediate between the supersonic and hypersonic simulations. The Reynolds numbers quoted in Table 1 are based on the distance downstream of the leading edge of the flat plate at which the oblique shock would impinge on the lower boundary in the absence of the boundary-layer. This distance is designated as x_0.

The boundary conditions applied differed between the supersonic and hypersonic simulations. For the supersonic cases (5 and 6), velocity and temperature boundary-layer profiles were prescribed at the inlet plane. These were generated by a separate self-similar compressible laminar boundary-layer analysis under the given freestream flow conditions (White, 1974). An adiabatic no-slip boundary condition was applied at the lower solid boundary.

For the hypersonic cases (1 - 4) uniform inflow conditions were used, except for the point at the solid wall where a no-slip condition was applied. In this way, the boundary-layer growth from the leading edge of the flat plate was simulated and the effects of viscous interaction near the leading edge of the flat plate were thus automatically taken into account, these being much more significant in the hypersonic cases. An isothermal cold wall ($T_w = 300$K) no-slip condition was applied at the lower solid boundary so that the wall heat-flux variation could be investigated.

In all cases a characteristic boundary condition was used at the outlet plane to minimize any reflected waves. At the upper computational boundary, freestream quantities were given in front of the oblique impinging shock-wave. The latter was introduced at a given location by applying the exact shock jump properties corresponding to a particular wedge angle, which were calculated analytically. The test gas considered was air, except for the $M_\infty = 6.85$ cases (3 and 4), for which it was pure nitrogen.

2.2 Grid and grid refinement

The grids employed in this study had a uniform spacing in the streamwise (x-) direction, but a non-uniform spacing in the wall-normal (y-) direction, with clustering towards the wall in order to capture better the boundary-layer gradients. A conformal, orthogonal mapping was applied to the computational domain to effect the clustering and the clustering parameter was varied in order to optimise the grid. This proved to be quite difficult for this configuration, as it is necessary not only to capture the gradients in properties within the boundary-layer, but also to resolve correctly the oblique impinging and reflected shocks.

Sensitivity of the numerical solution to the grids employed was investigated systematically for particular test cases. For the supersonic cases the baseline grid had 151 points in the x-direction and 128 points in the y-direction. With this grid and the particular clustering parameter employed there were approximately 20$\sim$30 points lying within the boundary-layer at the inlet plane. Test simulations were also carried out separately with 50% extra cells in the x- and y-directions. The results obtained were almost identical to those obtained with the baseline grid, indicating that a near grid-independent solution had been obtained.

Grid refinement and optimisation for the hypersonic cases was rather more challenging. It is thought that this was due to the difficulty in simulating accurately the initial boundary-layer growth near the leading edge of the plate, particularly as this is subject to the effects of viscous interaction. This will be discussed further in section 3.2. Ultimately an optimised grid was derived, comprising 128 $\times$ 192 points in the x- and y-directions respectively. With this grid typically about 40 - 60 points lay within the boundary-layer just upstream of the interaction. This grid was used as a baseline but, again, test simulations were carried out with 50% extra points in, separately, the x- and y-directions. Except near the leading edge of the plate these produced negligible changes compared with the baseline case, which was therefore considered to produce a near grid-independent solution.

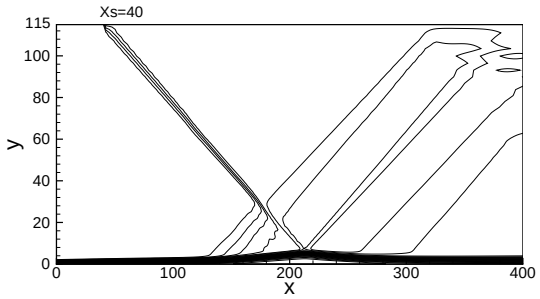

Figure 2: Mach number contours for $M_\infty = 2.0$ (case 6) with $p_3/p_1 = 1.40$.

3. Results

Oblique SBLI simulations were carried out for the range of conditions described in Table 1. In the following sections, particular attention is drawn to the simulations at $M_\infty = 2.0$ and $M_\infty = 7.87$, and the results obtained are compared with available experimental data at these two conditions. An attempt is then made to correlate data concerning certain features of the flowfield, using parameters that have been proposed previously by Katzer (1989), who derived them from the earlier work by Chapman *et al.* (1957). Here we extend the use of these parameters to higher Mach numbers in order to determine whether, or not, the flowfield under these conditions behaves according to the *free interaction* concept.

3.1 Simulations at $M_\infty = 2.0$

Figure 2 shows Mach number contours from case 6 with $p_3/p_1 = 1.40$. The incoming oblique shock follows the pre-defined shock angle ($\beta = 32.58^o$) and impinges on to the middle of the lower computational boundary, as required. In this case the impinging shock is sufficiently strong to cause the boundary-layer to separate. The simulations reproduce the main features as illustrated in Fig. 1 and are in agreement with the experimental observations. Some reflected waves appear around the upper/outflow corner of the computational boundary, which is due to the fixed flow properties used for the upper boundary after the shock. Similar reflected waves also occurred in the simulation of Wasistho (1998) for the same configuration. These features do not influence the flow near the solid boundary.

Figures 3 a) and b) show a comparison of the wall pressure and skin friction coefficient (C_f) for the above case with previous simulations (Katzer, 1989 and Wasistho, 1998) and experiment (Hakkinen et al., 1959). The wall pressures have been normalised by the freestream pressure at the inflow plane whereas C_f is defined conventionally from the wall shear stress. It is clear that, as the boundary-layer thickens and separates due to the shock impingement the wall pressure rises and reaches a plateau before increasing again at re-attachment. Simultaneously, the skin friction reduces and becomes negative (indicating separation and recirculation). A secondary minimum in C_f is also observed just ahead of the rise associated with re-attachment. These variations are typical of a laminar separation due to shock/boundary-layer interaction. They are in agreement with the previous numerical results and match fairly well the experimental results obtained for this configuration, particularly for the pressure variation. However, compared with the experimental data, the skin friction near re-attachment is under-predicted by all of the numerical simulations.

The effect of varying the impinging shock strength (and hence the overall pressure ratio) was explored. A sub-domain of $x = [100, 300]$ and $y = [0, 10]$ is used for plotting streamlines. Figure 4 a) shows the streamline traces for a weak impinging shock ($p_3/p_1 = 1.25$). In this case a small symmetric separation bubble is formed around the impingement point. The separation bubble increases in size as the shock strength is increased (see Fig. 4 b), c)) and becomes asymmetric in shape. For the strongest interaction illustrated ($p_3/p_1 = 1.65$) a small secondary vortex embedded inside the primary vortex is also evident. This also grows in size as the impinging shock strength is further increased. Note that streamline traces for $p_3/p_1 = 1.86$ case is not shown here. These results agree with those of Shen *et al.* (2000), who used a different numerical approach for the same configuration. Figure 5 compares the wall pressure and

skin friction coefficient distributions for the cases illustrated in Fig. 4. The pressure distributions illustrated in Fig. 5 a) indicate that there is no clear pressure plateau for weak interaction case, but the plateau develops as the impinging shock strength is increased. The plateau pressure increases slightly as the shock strength is increased, whereas the pressure at re-attachment rises sharply.

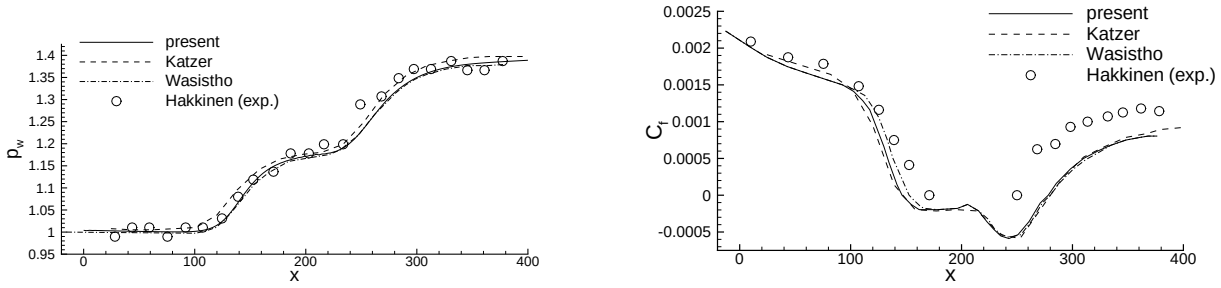

Figure 3: Comparison of simulations and experiment for $M_\infty = 2.0$ and $p_3/p_1 = 1.40$. a) wall pressure distributions, b) skin friction distributions.

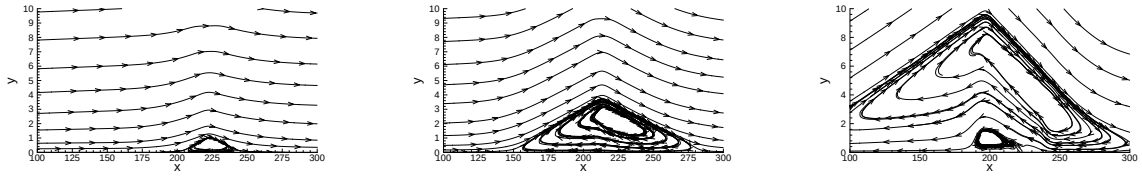

Figure 4: Streamline traces for $M_\infty = 2.0$ inflow. a) $p_3/p_1 = 1.25$, b) $p_3/p_1 = 1.40$, c) $p_3/p_1 = 1.65$.

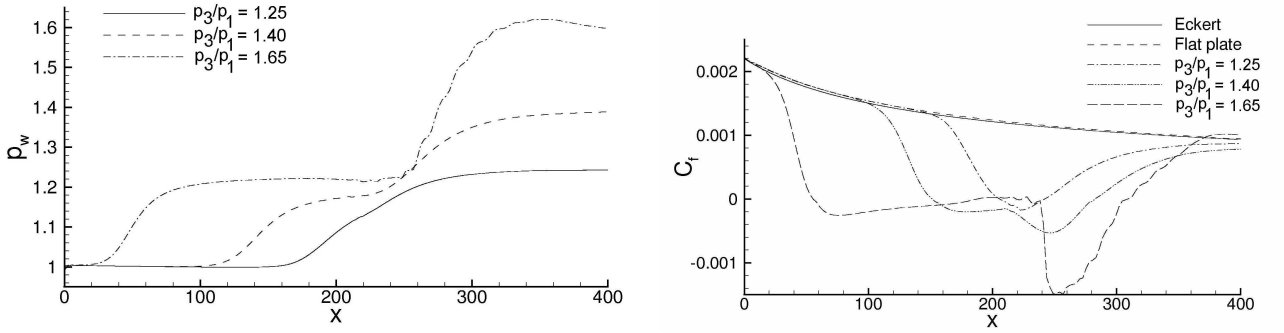

Figure 5: Comparison of case 6 at different overall pressure ratios. a) wall pressure distributions, b) skin friction distributions.

Figure 5 b) shows the corresponding skin friction coefficient (C_f) distributions. Flat plate results obtained from theory via the reference temperature method of Eckert (1955) and by numerical simulation are also plotted for reference. The latter agree well, again confirming that the inflow conditions and the undisturbed boundary-layer growth are simulated correctly. It is clear that, with shock impingement, the flow separation increases from incipient to extensive in size. The skin friction distribution for the strongest shock case illustrated confirms the presence of the secondary vortex. In these supersonic simulations, the shear stress near re-attachment rises to levels similar to those in the undisturbed flow.

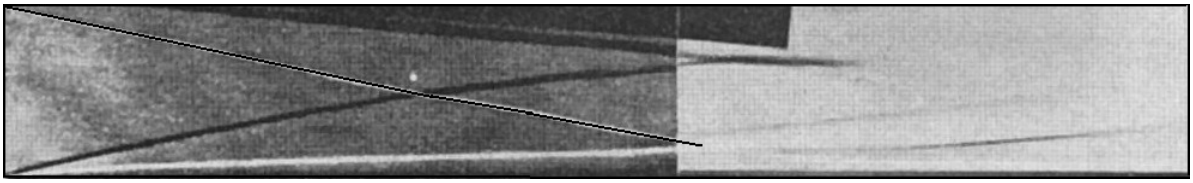

(a)

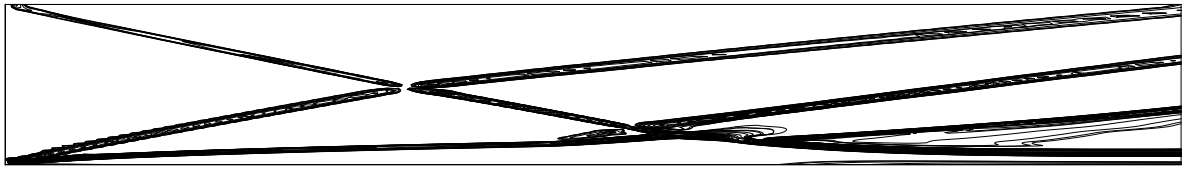

(b)

Figure 6: $M_\infty = 7.73$ (case 2) at a wedge angle of 5^o. a) Schlieren photograph, b) Density gradient contours.

3.2 Simulations at $M_\infty = 7.73$ and 7.87

Simulations were also carried out at $M_\infty = 7.73$ and 7.87 (see Table 1), and the results compared with experimental data obtained by Kaufman and Johnson (1974) at these conditions to ascertain the validity of the present numerical method for oblique shock SBLIs in the hypersonic regime.

Figure 6 a) shows the schlieren image obtained by Kaufman and Johnson for $M_\infty = 7.73$) with a wedge angle of 5^o (shock angle $\beta = 11.08$, $p_3/p_1 = 5.56$). The Reynolds number Re_{x_0} was 0.46×10^6. The rear of the wedge shock generator is visible at the top left of the image; the impinging shock emerging from the top left hand corner is also visible (note: the image has been enhanced to make this feature visible as a faint black line). On the lower boundary, the bow shock growing from the leading edge of the plate is clearly evident, along with the edge of the boundary-layer growing behind it. Although the flat plate is at zero incidence with respect to the freestream flow, the bow shock is generated as a result of viscous interaction with the developing boundary-layer.

Further downstream, after the impinging shock passes through the bow shock (with only slight refraction) it interacts with the boundary-layer, causing it to separate. Although the features in this region are not well-defined, a separation shock and re-attachment shock can just be observed, along with the re-attaching boundary-layer.

Figure 6 b) is the equivalent image obtained from the numerical simulation, plotted as contours of density gradient. All of the flow features described above are visible and appear to match well with the experimental image, and are similar to those sketched in Fig. 1.

Figure 7 illustrates the surface pressure and heat-flux distributions and compares the numerical and experimental results for this case. In Fig. 7 a) the pressure has been normalised by the freestream value at the inlet plane whereas, in b), the dimensional value of the heat transfer coefficient (defined conventionally from the wall heat-flux and the adiabatic wall temperature) is plotted. In both the x-axis corresponds to the distance from the leading edge of the flat plate, in millimetres.

Considering first the pressure distribution, the agreement between the experimental and numerical results appears to be rather poor. The distribution obtained via the numerical simulation is similar to that described earlier for the supersonic case, with a tendency towards a plateau in the separation zone. From streamline traces (not shown), the latter originates at about x = 175 mm and ends at about x = 300 mm. In the experimental case, the initial rise in pressure marking the onset of the interaction occurs much further downstream (x$\approx$200 mm) and the overall pressure rise measured is much less than that predicted numerically, although it follows a similar variation.

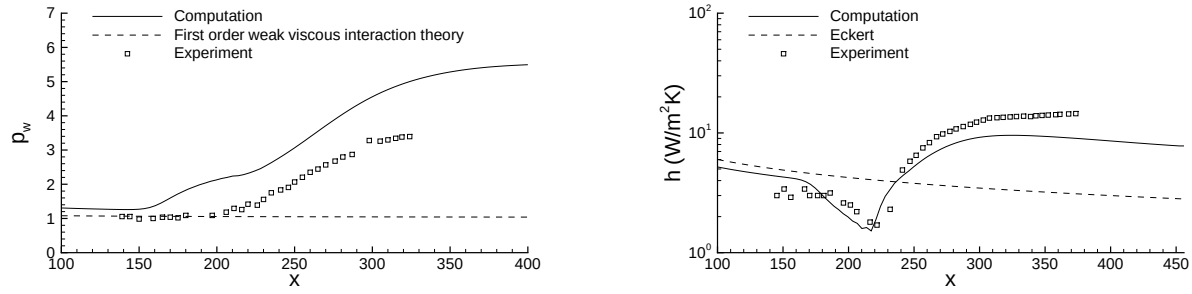

Figure 7: $M_\infty = 7.73$ (case 2) at a wedge angle of 5^o. a) wall pressure distributions, b) heat-flux distributions.

Also plotted in Fig. 7 a) is a curve corresponding to the pressure variation predicted for the undisturbed flow according to first order interaction theory (Anderson 1989). This suggests that viscous interaction effects are not strong under these conditions. In contrast, the numerical results indicate an enhancement in surface pressure of approximately 30% near the leading edge due to the presence of the bow shock. The fact that the experimental and numerically-generated schlieren images are almost identical suggests that the discrepancy might be due to the pressure measurements.

In Fig. 7 b) a similar discrepancy lies between the experimental and numerical data (note that the heat transfer coefficient has been plotted using a logarithmic scale). Again the numerical values exceed the experimental data in the undisturbed region and the onset of the interaction (indicated by the sudden reduction in heat-flux as the boundary thickens and separates) occurs further upstream numerically than was observed experimentally. The most notable difference compared with the pressure distribution, however, is that the heating levels measured experimentally near the re-attachment region exceed those predicted numerically.

For comparison, the theoretical heating distribution obtained for the undisturbed flat plate via the reference temperature method of Eckert (1955) is also plotted. Both the numerical and experimental results indicate lower heating levels in the undisturbed region compared with the Eckert prediction. In the numerical case, it is suspected that the grid is insufficiently fine to resolve adequately the temperature gradients in the boundary-layer near the leading edge, since further grid refinement does improve the agreement in this region. However, there is no obvious explanation for the comparatively low heat-fluxes measured experimentally in this region. This may indicate a systematic error in the heat-flux measurements, which makes the discrepancy between the experimental and numerical data in the re-attachment region even more remarkable. This will be discussed further in Section 4.

Similar results were obtained with simulations carried out with different wedge angles (with correspondingly different pressure ratios), although it was noted that the onset of the interaction appeared to be in better agreement with the experimental observations at low wedge angles. A test case was also carried out at a higher Reynolds number (1.48×10^6), at $M_\infty = 7.87$ and with $p_3/p_1 = 5.41$ (case 1). Again similar results were obtained with similar discrepancies between the measured and predicted pressure and heating distributions, although the difference between the measured and predicted heat-fluxes in the re-attachment region appeared to be slightly greater in the higher Reynolds number case.

3.3 Correlation of results

Numerous correlations derived from the *free interaction* concept have been proposed. For the present cases, the correlations used by Katzer (1989) were applied. He numerically studied two-dimensional supersonic SBLIs in a similar configuration to the present case under the influence of different Mach numbers ($1.4 \leqslant M_\infty \leqslant 3.4$), Reynolds numbers ($0.1 \times 10^6 \leqslant R_{e_{x_o}} \leqslant 0.6 \times 10^6$) and (weak) shock strengths on an adiabatic flat plate. In particular, he confirmed that the wall shear stress at the beginning of the interaction region and the Mach number at the edge of the boundary-layer govern the separation and plateau pressures. In this work we also consider hypersonic SBLIs with isothermal (cold) walls (see Table 1).

Figure 8 shows the pressure coefficients, c_p, at the separation point and in the plateau region of the present cases, plotted against the correlation parameter $(c_{f_1}/\sqrt{(M_1^2-1)})^{0.5}$ proposed by Katzer. The wall skin friction coefficient is obtained from a modified Blasius expression, $c_{f_1} = 0.664/\sqrt{Re_{x_1}/C}$, where x_1 is the position at the beginning of the interaction region and C is the Chapman-Rubesin constant (defined as $C = \sqrt{(\mu_w T_\infty)/(\mu_\infty T_w)}$).

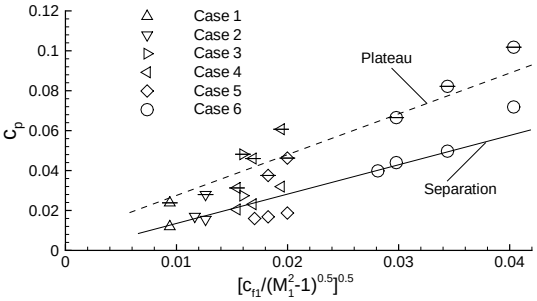

Figure 8: Pressures at separation points and plateau regions, with (*straight line*) for separation and (*dotted line*) for plateau. Pressures at plateau have short horizontal lines in their symbols.

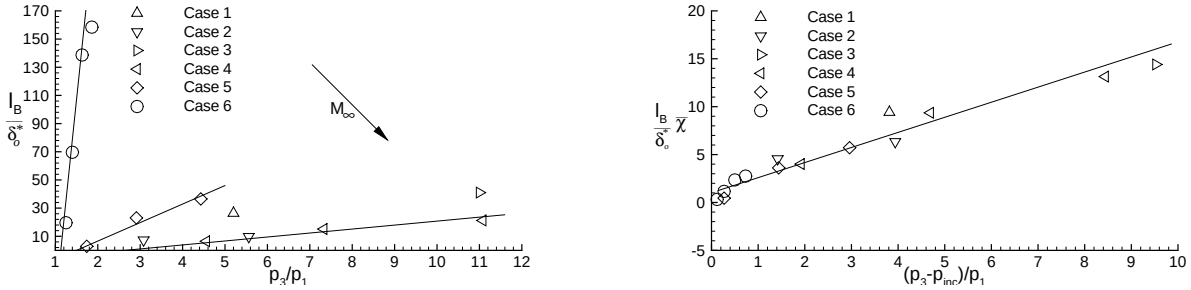

Figure 9: (**a**) Influence of the Mach number and shock strength. (**b**) Correlation for the separation bubble length.

The gradients (slopes) of the best-fit straight lines drawn through the data in Fig. 8 are 1.40 and 2.43 for the separation and plateau pressure, respectively. These gradients are in good agreement with experimental and numerical results cited by Katzer over a smaller range of Mach numbers. The scatter of separation and plateau pressure data about the best-fit lines are greatest for the strong shock simulation of cases 4 and 6. It is important to note that all of Katzer's data, which correlated better than the present data, concern weak interactions. Fig. 8 clearly indicates that as the Mach number is increased the c_p at separation and in the plateau region decreases. Note that, because $c_p = 1/M_\infty^2[(p/p_1) - 1]$, the actual pressure ratios at separation (p_s) or in the plateau region (p_p) increase with Mach number.

Figure 9 a) shows the influence of Mach number and shock strength on the length of the separation bubble l_B, the latter being normalised by δ_o^* (displacement thickness of an undisturbed boundary-layer at the position of impingement point, x_o). It can be seen that the bubble length increases with increasing shock strength, p_3/p_1, as described earlier. The intersections of the plotted lines with the abscissa show the separation occurs only when the shock strength is larger than a certain threshold value, p_{inc}, which appears to increase with increasing Mach number. It would also appear that the separation length decreases (for a given overall pressure ratio) with increase in Mach number. There is also a suggestion that increasing the Reynolds number increases the separation length, although with only two significant data points (at $M_\infty = 6.85$ and 7.87) it is difficult to be conclusive in this regard.

For his supersonic SBLI cases (with relatively low overall pressure ratio, p_3/p_1, or shock strength), Katzer showed that the normalised separation length could be correlated in terms of the overall pressure rise $(p_3 - p_{inc})/p_1$ by including the viscous interaction parameter, $\bar{\chi} = M_\infty^3 \sqrt{C/R_{e_{x_o}}}$. The data obtained from the present simulations over a wide Mach number range and with relatively high overall pressure ratios, as plotted in Fig. 9 b), also appear to be well correlated by this parameter (Fig. 9 b). However, the gradient of the straight line of best fit that correlates the present data in Fig. 9 b) is about 1.8, whereas that for Katzer's data was 4.4. Close inspection of the present case 6 data does indicate that the local gradient at low overall pressure ratios is higher and close to that of Katzer, but evidently that does not extend to higher Mach number cases. Perhaps instead of a straight line it would be more appropriate to correlate the data using a power-law function, as suggested by Kaufman and Johnson (1974). Nevertheless, the

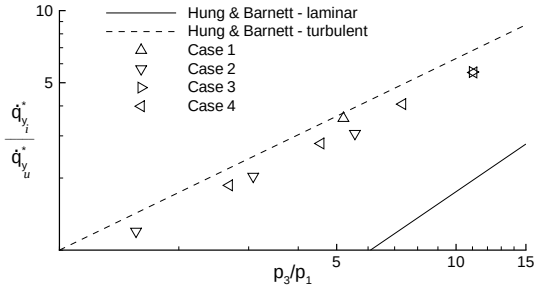

Figure 10: Peak heating correlation. Turbulent (*dotted line*) and laminar (*straight line*) peak heating correlations.

results from the present simulations suggest that the hypersonic flowfields do conform to the *free interaction* concept.

The prediction of the peak heating rates in the re-attachment region represents a practical engineering problem. Hung and Barnett (1973) proposed correlations for peak heating rates in laminar, transitional and turbulent interactions induced by incident shocks or a compression corner. The correlation comprises a power-law relation between the ratio of the peak values of the pressure and heating to their undisturbed values that is a function of the boundary-layer state in the vicinity of the interaction.

Figure 10 compares the heating data from the present numerical simulations for peak heat-flux, q^*_y, with Hung and Barnett's laminar and turbulent correlation plotted in term of the overall pressure ratio, p_3/p_1. Subscripts i and u denote interaction and undisturbed regions, respectively. It can be seen that the present data do comply with a power-law relationship, with an exponent of 0.8, but lie fairly close to the turbulent correlation. However, as the simulation code used is purely laminar, the better agreement with the turbulent correlation in Fig. 10 is questioned and may be fortuitous. The effect of a small changes in Reynolds number seem to be only slight.

4. Discussion and Concluding Remarks

Oblique SBLI simulations have been carried out in the present work that cover a wide range of Mach numbers and overall pressure ratios. Features such as the separation and plateau pressures, and the length of the separation bubble, were correlated in terms of parameters developed previously by other researchers for supersonic SBLIs, but have here been extended into the hypersonic regime. The results obtained at $M_\infty = 2.0$ agree well with simulations carried out previously by other workers, and agree reasonably well with the available experimental data. In contrast, the agreement with experimental data at $M_\infty = 7.73$ and 7.87 is relatively poor. In particular, the pressures in the interaction region are over-predicted and the wall heat-fluxes are under-predicted.

Similar observations have been made by other researchers who have carried out hypersonic 2-D SBLI simulations. For example, Amaratunga *et al.* (1998) and Navarro-Martinez (2002) have attempted to simulate the flat plate-compression ramp experiments carried out by Smith (1993), in which unexpectedly high heat-fluxes were observed in the re-attachment region on the compression ramp. From this work it has become clear that 2-D laminar simulations generally over-predict the separation length and under-predict the heat-flux at re-attachment. Navarro-Martinez has carried out further 3-D simulations that allow for the effects of lateral venting from the separation bubble. This has partially resolved the issue concerning over-prediction of the separation length, but has had relatively little effect on the re-attachment heat-flux. Localised 3-D effects (Görtler vortices) have also been shown to produce local streamwise increases in heat-flux in the re-attachment region, but again this has failed to resolve fully the discrepancy between the measured and predicted heat-fluxes.

In the present case, it is quite likely that the experiments of Kaufman and Johnson were influenced by lateral venting, since the aspect ratio of the flat plate they employed was rather small(0.38). This may well help explain the observed differences between the measured and predicted surface pressures and the location of the onset of the interaction region. It is probable, however, that - just as in the compression ramp case - the observed discrepancy in the heating distribution is too large to be accounted for solely by the influence of 3-D effects.

Kaufman and Johnson admit the possibility of the separated shear layer undergoing transition in some of their experiments; if so this would have the observed effect of reducing the separation bubble length and increasing the heat-flux at re-attachment. In order to test this hypothesis, further 3-D unsteady simulations are presently underway to investigate the propensity of the boundary-layer, or separated shear layer, to undergo transition in response to small, artificially applied perturbations. The results of these simulations will be reported at a future date.

5. Acknowledgements

This work was carried out with support from the Engineering and Physical Sciences Research Council (EPSRC) and the Defence Science and Technology Laboratory (DSTL).

6. References

Adamson, T.C. Jr., and Messiter, A.F. (1980) Analysis of two-dimensional interactions between shock waves and boundary layers. Ann. Rev. Fluid Mech. 12:103-138.

Amaratunga, S., Tutty, O.R., and Roberts, G.T. (1998) Numerical predictions of hypersonic flow over a 2-D compression ramp. J.Spacecraft and Rockets, vol. 35, no. 2, Mar-Apr 1998, pp. 230-232.

Anderson, J.D. (1989) Hypersonic and high temperature gas dynamics. McGraw-Hill.

Bura, R.O., Roberts, G.T., Sandham, N.D. and Yao, Y.F. (2001) Simulation of hypersonic shock-wave/boundary-layer interactions. Proc. of the 23rd Int. Symp. on Shock Waves (ISSW23), Forth Worth, Texas, USA, pp.1371-1377. Edited by Frank K. Lu.

Chapman, D.R., Kuehn. D.M. and Larson, H.K. (1957) Investigation of separated flows in supersonic and subsonic streams with emphasis on the effect of transition. NACA TN 3869. Also 1958. NACA TR 1356.

Degrez, G., Boccadoro, C.H. and Wendt, J.F. (1987) The interaction of an oblique shock wave with a laminar boundary layer revisited. An experimental and numerical study. Journal of Fluid Mechanics, 177:247-263.

Delery, J.M. and Panaras, A.G. (1996) Shock Wave Boundary-layer Interactions in High Mach Number Flows, AGARD Advisory Report No.319 (AGARD AR-319), Vol.1, pp.2-1 to 2-61.

Delery, J.M. (1999) Shock phenomena in high speed aerodynamics: still a source of major concern. The Aeronautical Journal, 1:19-34.

Dolling, D.S. (2001) Fifty years of shock-wave/boundary-layer interaction research: what next? AIAA Journal 39(8):1517-1531.

Domröse, U., Krause, E. and Meinke, M. (1996) Numerical Simulation of Laminar Hypersonic Shock-Boundary Layer Interaction. Z. Flugwiss. Weitraumforsch., 20(2):89-94.

Eckert, E.R.G. (1955) Engineering relations for skin friction and heat transfer to surfaces in high velocity flows. Journal of the Aeronautical Sciences, 22:585-587.

Hakkinen, R.J., Greber, I., Trilling, L. and Abarbanel, S.S. (1959) The interaction of an oblique shock wave with a laminar boundary layer. NASA Memo 2-18-59 W.

Hankey, W.L. and Holden, M.S. (1975) Two-Dimensional Shock Wave - Boundary Layer Interactions in High Speed Flows. AGARDograph No.203.

Henckels, A., Kreins, A.F. and Maurer, F. (1993) Experimental Investigations of Hypersonic Shock-Boundary Layer Interaction. Z. Flugwiss. Weitraumforsch., 17(2):116-124.

Hodge, B.K. (1977) Prediction of Hypersonic Laminar Boundary-Layer/Shock-Wave Interactions. AIAA Journal, 15(7):903-904.

Holden, M.S. (1978) A Study of Flow Separation in Regions of Shock Wave-Boundary Layer Interaction in Hypersonic Flow. AIAA Paper 78-1169.

Holden, M.S. (1986) A Review of Aerothermal Problems Associated with Hypersonic Flights. AIAA Paper 86-0267.

Hung, F.T., and Barnett, D.O. (1973) Shockwave-boundary layer interference heating analysis. AIAA paper 73-238.

Issa, R.I. and Lockwood, F.C. (1977) On the Prediction of Two-Dimensional Supersonic Viscous interactions Near Walls. AIAA Journal, 15(2):182-188.

Katzer, E. (1989) On the lengthscales of laminar shock/boundary-layer interaction. Journal of Fluid Mechanics, 206:477-496.

Kaufman, L.G.II and Johnson, C.B. (1974) Weak Incident Shock Interactions with Mach 8 Laminar Boundary-Layers. NASA TN D-7835.

Korkegi, R.H. (1971) Survey of Viscous Interactions Associated with High Mach Number Flight. AIAA Journal, 9(5):771-784.

Kreins, A.F., Henckels, A. and Maurer, F. (1996) Experimental Studies of Hypersonic Shock Induced Boundary Layer Separation. Z. Flugwiss. Weitraumforsch., 20(2):80-88.

Liepmann, H.W. (1946) The interaction between boundary layer and shock waves in transonic flows. Journal of Aerospace Sciences, 13(12):623-638.

Navarro-Martinez, S. (2002) Numerical simulation of laminar flow over hypersonic compression ramps. University of Southampton PhD thesis.

Needham, D.A. and Stollery, J.L. (1966) Boundary-layer Separation in Hypersonic Flow. AIAA Paper 66-455.

Sandham, N.D., Li, Q. and Yee, H.C. (2002) Entropy splitting for high-order numerical simulation of compressible turbulence. Journal of Computational Physics, 178(2):307-322.

Shen, Y. Wang, R. and Liao H. (2000) A new numerical study of the shock/boundary-layer interaction. Int. J. Numer. Methods in Fluids, 33:23-34.

Smith, A.J.D. (1993) The dynamic response of a wedge separated hypersonic flow and its effects on heat transfer. University of Southampton PhD thesis.

Wasistho, B. (1998) Spatial direct numerical simulation of compressible boundary layer flow. Ph.D thesis, University of Twente, Netherlands.

White, F.M. (1974) Viscous Fluid Flow. McGraw-Hill.

Yao, Y.F., Lawal, A.A., Sandham, N.D., Wolton, I.C., Ashworth, M. and Emerson, D.R. (2000) Massively parallel simulation of shock/boundary-layer interactions. Proc. of Inter. Conf. of Applied Computational Fluid Dynamics, Beijing, China, pp.728-735.

Yao, Y.F., Bura, R.O., Sandham, N.D and Roberts, G.T. (2002) Time-accurate simulation of supersonic and hypersonic laminar shock/boundary-layer interactions In Proc. CEAS Aerospace Aerodynamics Research Conference, Cambridge, pp.373-386.